



Hydrological regime shifts in Sahelian watersheds: an investigation with a simple dynamical model driven by annual precipitation

Erwan Le Roux¹, Valentin Wendling², Gérémy Panthou³, Océane Dubas³, Jean-Pierre Vandervaere³, Basile Hector³, Guillaume Favreau³, Jean-Martial Cohard³, Caroline Pierre⁴, Luc Descroix⁵, Eric Mougin⁶, Manuella Grippa⁶, Laurent Kergoat⁶, Jérôme Demarty⁷, Nathalie Rouche⁷, Jordi Etchanchu⁷, and Christophe Peugeot⁷

¹IMT Atlantique, Lab-STICC, UMR CNRS 6285, 29238, Brest, France

²HydroSciences Montpellier (Univ. Montpellier, IMT Mines Ales, CNRS, IRD) Ales, France

³Institut des Géosciences de l'Environnement (Univ. Grenoble Alpes, INRAE, CNRS, IRD, Grenoble INP), Grenoble, France

⁴Institut d'Ecologie et des Sciences de l'Environnement de Paris (CNRS, Sorbonne Univ., Univ Paris Est Creteil, IRD, INRAE, Univ. de Paris) Paris, France

⁵Patrimoines locaux, Environnement et Globalisation (MNHN, IRD, CNRS), Paris, France

⁶Géosciences Environnement Toulouse (CNRS, IRD, UPS, CNES) Toulouse, France

⁷HydroSciences Montpellier (IRD, Univ. Montpellier, CNRS) Montpellier, France

Correspondence: Erwan Le Roux (erwan.le-roux@imt-atlantique.fr)

Abstract. The Sahel, the semi-arid fringe south of the Sahara, experienced severe meteorological droughts in the '70s-'80s. Since these droughts, watersheds in the Central Sahel have experienced an increase in the annual runoff coefficient (annual runoff normalized by annual precipitation). We hypothesize that these increases correspond to regime shifts. To investigate the timing of these regime shifts, we introduce a lumped model that represents feedbacks between soil, water and vegetation at the watershed scale and the annual time step. This model relies on runoff coefficient as a constraint for the state variable and precipitation as unique external forcing. Four watersheds (Gorouol, Dargol, Nakanbé and Sirba), with pluri-decadennial observations ('50s-2010s), are modeled. For each watershed, one million parameterizations of this model are sampled and run, and an ensemble of one thousand best parameterizations is selected based on observed runoff coefficients. Our results show that this model can reproduce the trend of runoff coefficients. For all watersheds, almost all selected parameterizations from the ensemble are bistable, and can be utilized to define two alternative runoff coefficient regimes: a low and a high regime. Most ensemble members undergo regime shifts: simulated runoff coefficients belong to the low regime in 1965 and to the high regime in 2014. Finally, we find that the year of the regime shift, defined as the first year with more than 50% of ensemble members in the high regime, was 1968, 1976, 1977, 1987 for the Gorouol, Dargol, Nakanbé and Sirba watershed, respectively. This article proposes several simple ideas toward improving the modelling and characterization of hydrological regime shifts.

1 Introduction

Complex dynamical systems (ecosystems, climate system) can experience shifts to a contrasting regime (Scheffer et al., 2001). Such regime shifts correspond to the transition from an attraction basin to an alternative attraction basin. Regime shifts occur when a tipping point is crossed, i.e. a critical value beyond which a system switches to the alternative basin, often abruptly



and/or irreversibly (IPCC, 2023). In the literature, tipping points often denote critical thresholds of the external condition of the dynamical system (Armstrong McKay et al., 2022). However, we note that a tipping point can also refer to a critical level of noise in the state space or a critical rate of change in the external condition (Lenton, 2011; Ashwin et al., 2012).

In hydrological science, better accounting for regime shifts remains a challenge (Blöschl et al., 2019; van Hateren et al., 2023) that could lead to a new paradigm: accounting for non-stationary changes (Milly et al., 2008) and also for potential abrupt and/or irreversible changes (Fowler et al., 2022a). Some approaches rely solely on data to emphasize multiple lines of evidence that could be related to a regime shift (Zipper et al., 2022; Fowler et al., 2022b; Rahimi et al., 2023; Goswami et al., 2024). In particular, several studies highlight a shift of watersheds toward lower streamflow during drought due to shifts in the relationships between surface water and groundwater (Saft et al., 2015; Peterson et al., 2021; Fowler et al., 2022a; Liu et al., 2023). Other approaches combine existing data with a dynamical model to analyze potential regime shifts: Wendling et al. (2019) modeled in the Northern Mali a shift from a high-vegetation/low-runoff regime to a low-vegetation/high-runoff regime, while Dijkstra et al. (2019) used an idealized model to show that a shift from a low to a high sediment concentration regime may occur in the Ems River assuming low river discharge and increasing channel depth. Spatial models of dryland vegetation have also been used to study eco-hydrological regime shifts (Van Nes and Scheffer, 2005; Mayor et al., 2019; Kéfi et al., 2024).

This study focuses on the Sahelian hydrological paradox (Mahe et al., 2005; Descroix et al., 2009). In the Central Sahel (Mali, Burkina Faso, Niger), annual runoff coefficients (annual runoff normalized by annual precipitation) of watersheds increased during the major meteorological droughts in the '70s-'80s and surprisingly kept increasing after them. This paradox is attributed to the hydrological effect of land clearing (Leblanc et al., 2008; Favreau et al., 2009) which favors soil crusting and thus Hortonian surface runoff (Horton, 1933), the dominant runoff generation process in the region (Casenave and Valentin, 1992). In the northernmost areas where rainfed agriculture is not possible, the paradox is attributed to drought-induced vegetation dieback (Hiernaux et al., 2009; Gardelle et al., 2010; Gal et al., 2017).

In this study, for every watershed, we assume that this Sahelian hydrological paradox corresponds to a hydrological regime shift from a low to a high runoff coefficient regime, and ask: when did the shift between these two regimes occur ?

Answering this question requires a dynamical model that can account for a hydrological regime shift of Sahelian watersheds. However, to our knowledge, such a model does not yet exist. To fill this gap, we build on previous work in ecological modelling (van Nes et al., 2014; Wendling et al., 2019) to develop a lumped dynamical model that can simulate these regime shifts. This model simulates annual runoff coefficient at the watershed scale and the annual time step, using annual precipitation as unique external forcing. This interpretable model incorporates feedbacks between vegetation dynamics and runoff generation. For four Sahelian watersheds, it is calibrated with an ensemble approach, using observations of precipitation and runoff coefficients.

Furthermore, to answer our question, we have to be able to quantitatively identify a regime shift. Regime shifts are often conceptualized with state values that remain equal to attractors, i.e. values asymptotically reached by the dynamical model (see Figure 2 of Scheffer et al., 2001). However, in our study, the model displays transient dynamics (Hastings et al., 2018; Feudel, 2023), where state values are sometimes far from attractors. In this context, we propose to quantitatively identify a regime shift based on a definition of regimes that involves splitting the state space into two regimes: a low and a high regime.



This paper is organized as follows. Section 2 presents our data. Section 3 develops our methodology. Results, discussions and conclusions are introduced in Sects. 4, 5 and 6, respectively.

55 2 Data

2.1 Sahelian watersheds

The four considered watersheds (Gorouol, Dargol, Sirba, Nakanbé), located in central Sahel (Fig. 1), are selected on the basis of their pluri-decennial observations. The first three are tributaries of the Niger River, and the last one feeds the Volta River. The climate of this semi-arid region is governed by the West African monsoon (Redelsperger et al., 2006; Lafore et al., 2011). Seasonal precipitation is provided by mesoscale convective systems between June and September. Intermittent rivers are supplied by surface runoff generated on hillslope during rainstorms. The study area is essentially rural: the north is dominated by natural pastures grazed by cattle, while the south contains a mosaic of savannahs and fields (rainfed and fallow), where scattered shrub and tree species persist (Tucker et al., 2023).

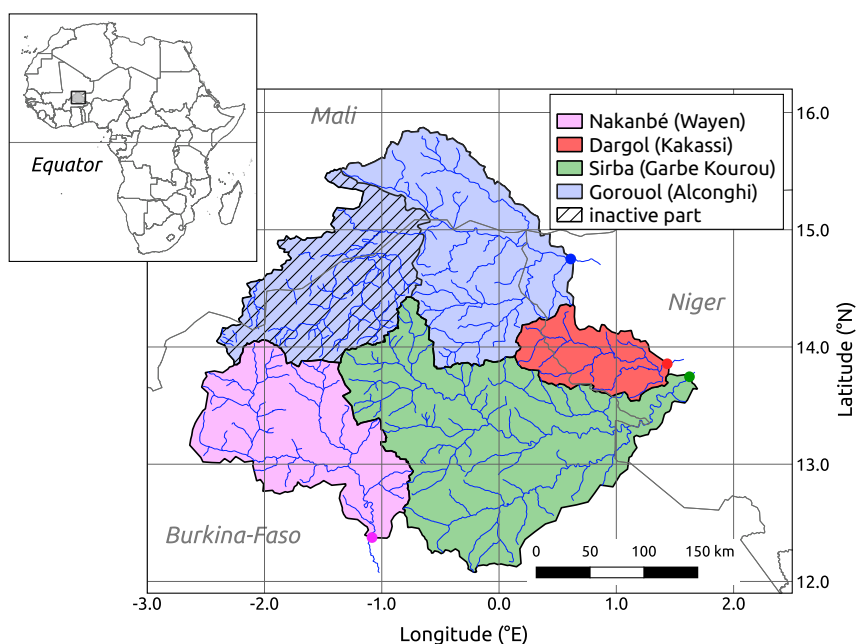


Figure 1. Location of the study area in Sub-Saharan Africa, and map of the four watersheds. The grey lines are the country borders. The large dots show the watershed outlet. The names of corresponding streamflow stations are in brackets in the legend. The upper Gorouol basin was inactive between the 1950s and the 2010s and does not contribute to the streamflow. Only the active sub-basin is considered.



2.2 Annual precipitation

65 Annual precipitation over each watershed are computed using the approach proposed by Panthou et al. (2018). First, for each gauge station of the watershed, annual precipitation series are obtained by summing daily precipitation for each year. Then, annual precipitation means and anomalies are both interpolated using two kriging methods. Finally, annual precipitation of the watershed is computed as the sum of these two interpolated fields (means and anomalies) averaged spatially over the watershed.

70 Figure 2a presents annual precipitation over four watersheds for the period 1956-2014. Past annual precipitation can be grouped in three main periods: wet during the '50s-'60s, followed by severe droughts which ended up in the mid-'90s, and recently a strong inter-annual variability where annual precipitation roughly equals the mean of the whole period.

2.3 Annual runoff coefficient

The annual runoff coefficient K (-), ranging between 0 and 1, is equal to the annual watershed outflow V (m^3) per unit of watershed area A (m^2), normalized by the annual precipitation P (mm): $K = \frac{V}{A \times P}$. Annual watershed outflow V (m^3) is calculated from the mean daily discharge Q ($m^3 s^{-1}$), in a hydrological year, starting on the first of March. For the Nakanbé watershed, we use discharges corrected for the effect of dams built in recent decades (Gbohoui et al., 2021). For the three other watersheds, discharges are merged from several robust databases: SIEREM (Boyer et al., 2006) and ADHI (Tramblay et al., 2021). We exclude years with more than 13 days of missing consecutive daily discharge values during the wet season (June-September). Otherwise, missing values are set to zero in the dry season, and linearly interpolated in the wet season. A sensitivity study (not shown) confirms that this interpolation has a limited effect on the mean annual discharge (bias < 10%).

80 Figure 2b presents the annual runoff coefficient series for each watershed. All watersheds have experienced a similar evolution toward higher annual runoff coefficients although the Northern watersheds display higher coefficients.

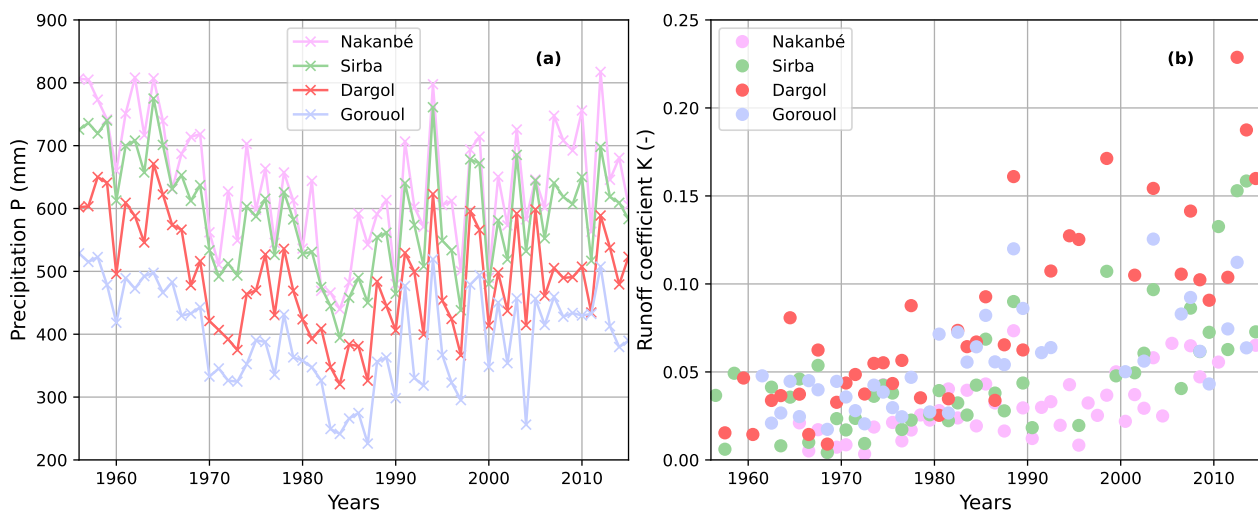


Figure 2. Observations of (left) annual precipitation and (right) annual runoff coefficient for the four watersheds between 1956 and 2014.



3 Methodology

All physical variables are defined at watershed scale and at annual time step, e.g. precipitation refers to annual precipitation of the watershed. Moreover, variables are denoted with uppercase letters, whereas parameters are written with lowercase letters.

3.1 Dynamical model

We develop a lumped dynamical model that simulates the runoff coefficient K of a watershed. This parsimonious model has a single external forcing, the precipitation P (mm), and a single state variable, the water holding strength S (-). S ranges from 0 to 1. The higher is S , the lower is K . In the model, S represents all physical mechanisms that hold water including low runoff connectivity, closed basins that retain water, or soil infiltration properties due to developed vegetation cover.

The proposed dynamical model is an extension at the watershed scale of a previous hillslope scale model (Wendling et al., 2019), inspired by ecological modelling (van Nes et al., 2014). Indeed, given the dominant role of vegetation in the Sahelian paradox, variations in S are assumed to be similar to those of a vegetation cover. In the model, S increases and decreases as a function of I (mm), an indicator of wetness representing the potential water for the vegetation, i.e. precipitation minus runoff.

Changes in the water holding strength S are modulated by a feedback loop (Fig. 3). S impacts directly the proportion of outflow water K , that indirectly affects the indicator of wetness I , which finally drives the growth and decays of S . Mathematically, changes in S are prescribed using a differential equation, where the time derivative $\frac{dS}{dt}$ is denoted as \dot{S} . The computation of \dot{S} can be decomposed into three steps (Eq. 1, Eq. 2, Eq. 3), schematically represented in Figure 3, and detailed below.

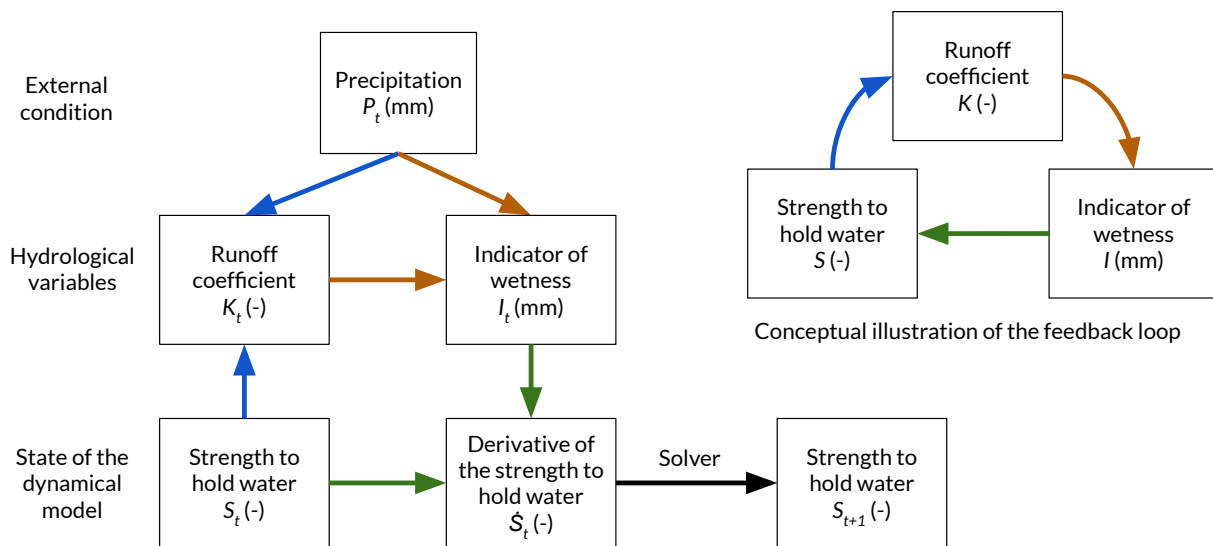


Figure 3. At every time t , the derivative of the water holding strength \dot{S}_t is computed in three steps: i) the runoff coefficient K_t is derived from the water holding strength S and the precipitation P (Eq. 1), ii) the indicator of wetness I_t is determined by the runoff coefficient K_t and the precipitation P_t (Eq. 2), iii) the derivative \dot{S}_t is calculated with the water holding strength S_t and the indicator of wetness I_t (Eq. 3).



First, we assume that the runoff coefficient K is a function of the water holding strength S and the precipitation P :

$$100 \quad K = f \times k_{max} \cdot \left(\frac{P^a}{P^a + C^a} \right)^b \quad \text{with } C = c_{min} + S \times (c_{max} - c_{min}) \quad (1)$$

where C (mm) is the water holding capacity; a (-), b (-), f (-), k_{max} (-), c_{min} (mm), c_{max} (mm) are positive parameters (Table 1). The runoff coefficient K is maximized when precipitation is extremely higher than the water holding capacity ($P \gg C$), i.e. when S is close to 0. Inversely, the runoff coefficient K is close to zero if $C \gg P$, i.e. when S is close to 1.

In the second step, the indicator of wetness I (mm) is derived from the precipitation P and the runoff coefficient K :

$$105 \quad I = P \cdot \left(1 - \frac{K}{f} \right) \quad (2)$$

Finally, we further assume that the derivative of the water holding strength \dot{S} can be calculated from S and I :

$$\dot{S} = \overbrace{r_g \cdot \frac{I}{I + i_g} \cdot S \cdot (1 - S)}^{(1)} - \overbrace{r_d \cdot \frac{i_d}{I + i_d} \cdot S}_{(2)} + \overbrace{\mu \cdot (1 - S)}^{(3)} \quad (3)$$

where r_g (year⁻¹), i_g (mm), r_d (year⁻¹), i_d (mm) and μ (year⁻¹) are positive parameters. Equation 3 contains a growth term (1) and a decay term (2), whose rates (r_g and r_d) are modulated by I . The balance between these terms depends on S and I , and determines the sign of the derivative of S , hence its variation. The third term of Eq. 3 is small and only prevents the unrealistic convergence to $S = 0$. It can be interpreted as the representation of physical processes that spontaneously increase the water holding strength such as sand deposits by the wind, and vegetation growth due to seeds imported.

3.2 Model calibration

For each watershed, the calibration of the dynamical model is performed using observed precipitations and runoff coefficients.

115 Formally, let $\theta = \{k_{max}, a, b, c_{min}, c_{max}, c_g, c_d, i_d, \mu, f\}$ denote a parameterization of the dynamical model, i.e. a set of parameters for the equations (Eq. 1, Eq. 2, Eq. 3). Calibrating a single optimal parameterization θ^* can be prone to equifinality, i.e. when different parameterization lead to similar results (Beven, 2006). This is one of the reasons why, for each watershed, we calibrate an ensemble of parameterizations. Following (Wendling et al., 2019), this ensemble is built in four steps:

1. 10⁶ parameterizations are sampled from a Latin hypercube sampling, using a uniform distribution over a large range of parameter values (Table 1). These ranges were adjusted through preliminary tests.
2. For each parameterization the trajectory of simulated water holding strength S is solved numerically, with a wrapper of the Fortran solver from ODEPACK Hindmarsh (1983), using observed precipitations as a forcing.
3. For each parameterization, the trajectory of simulated runoff coefficient K is inferred from S using Eq. 1.



125

4. The calibrated ensemble Θ^* is defined as the set of 1000 best parameterizations, $\Theta^* = \{\theta^{(1)}, \dots, \theta^{(1000)}\}$. The selection of best parameterizations is based on the root mean squared error between observed and simulated runoff coefficients.

Parameter	Description	Unit	Value/Range
r_g	Growth rate	y^{-1}	[0.2, 2.0]
r_d	Decay rate	y^{-1}	[0.5, 5]
i_g	Half-saturation constant for growth	mm	[150, 700]
i_d	Half-decay constant for decay	mm	[10, 200]
μ	Minimum growth rate	y^{-1}	[2e-3, 5e-3]
c_{min}	Minimum value of water holding capacity	mm	[0, 140]
c_{max}	Maximum value of water holding capacity	mm	[600, 800]
k_{max}	Maximum runoff coefficient	-	0.9
a	Shape parameter (steepness)	-	1.5
b	Scale parameter (inflection point)	-	8.0
f	Land fraction contributing to the discharge outlet	-	[0.1, 1]

Table 1. Parameters of the dynamical model: name, description, unit and value or range of values.

3.3 Bistable parameterizations

For each parameterization θ of the ensemble Θ^* , we compute its bifurcation diagram (Fig. 4). This diagram is a graph that associates each forcing value with the corresponding attractors of the dynamical model, i.e. the stable equilibrium states asymptotically reached by the model. Here, the attractors are calculated as the final value of S after a 10000-year simulation with a series of constant precipitation values between 1 and 2000 mm. Each simulation is initialized with two different states ($S = 0.01$ and $S = 0.99$), which can lead to the same attractor (monostability) or to two different attractors (bistability). We define that a parameterization θ is i) monostable if it has a single attractor for every precipitation value between 1 and 2000 mm ii) bistable if it has two attractors for at least one precipitation value.

Figure 4 illustrates the bifurcation diagram for a monostable and a bistable parameterization θ . In particular, Figure 4 (b) shows a bifurcation diagram containing a precipitation range with two attractors (roughly between 700 and 1500 mm). For any precipitation in this range, two S values can be reached asymptotically depending on the initial state value. We denote as lower and upper branch the lines formed by the lower and upper attractors, respectively. Sometimes, as exemplified in Figure 4 (b), there exists a range of values S between the lower and upper branches of the attractors. These state values may converge asymptotically toward either the upper or lower branch depending on the forcing precipitation value P .

Otherwise, the reason why we calculate attractors until 2000 mm, i.e. roughly two times the maximum observed precipitation (Sect. 2.2), is to assess what is the maximum precipitation value where the lower branch of attractors ends.

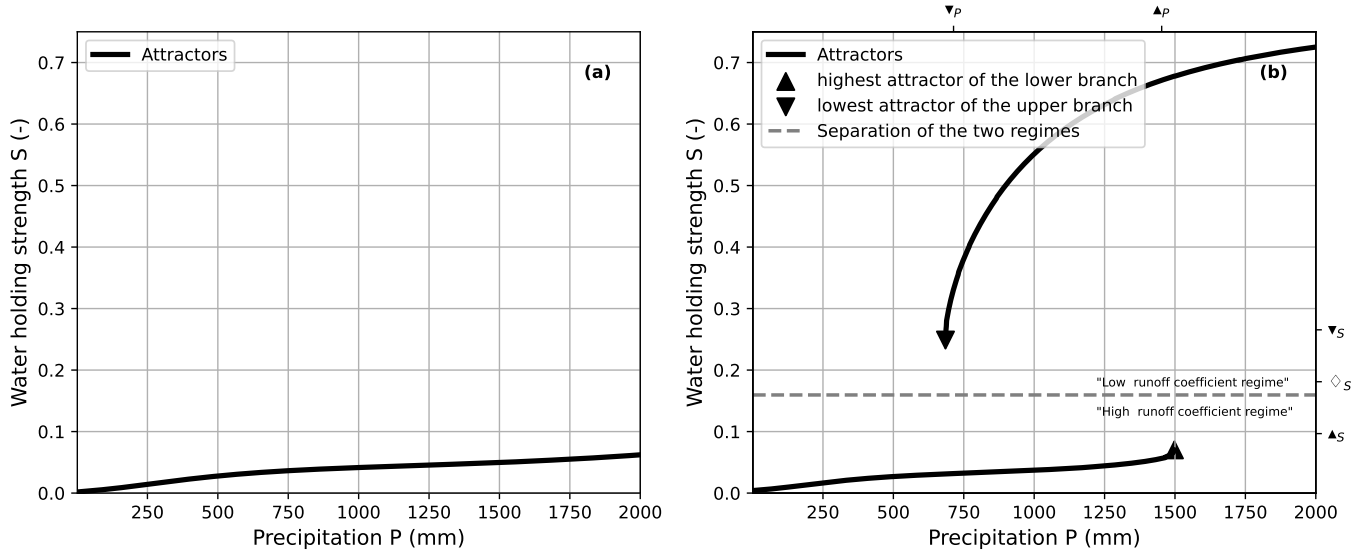


Figure 4. Bifurcation diagram of a (a) monostable (b) bistable parameterization θ for precipitation P between 1 mm and 2000 mm. Runoff coefficient regimes are defined for bistable parameterizations. The separation of the two regimes is the value \diamond_S , which is the mean between the highest attractor of the lower branch \blacktriangle_S and the lowest attractor of the upper branch \blacktriangledown_S . Associated precipitation values are \blacktriangle_P and \blacktriangledown_P .

3.4 Regime shift

Regimes and regime shifts are often conceptualized with state values that remain equal to attractors (Scheffer et al., 2001). However, many systems have transient dynamics, where state values remain far from attractors (Hastings et al., 2018). In these cases, regimes and regime shifts can be determined using quasi-static simulations, where the external forcing is changed infinitely slowly so that state values remain close to their attractors (Hankel and Tziperman, 2023). In our case study, due to the important variability of the external forcing (precipitation) such simulations are irrelevant. Thus, we propose a simple definition of regimes that separates in two regions the bifurcation diagram. Specifically, for each bistable parameterization θ , we define two regimes (the "Low runoff coefficient regime" and the "High runoff coefficient regime") as follows:

$$150 \quad \text{Regime}(S|\theta) = \begin{cases} \text{"High runoff coefficient regime", i.e. with low water holding strength, if} & S < \diamond_S = \frac{\blacktriangledown_S + \blacktriangle_S}{2} \\ \text{"Low runoff coefficient regime", i.e. with high water holding strength, if} & S \geq \diamond_S = \frac{\blacktriangledown_S + \blacktriangle_S}{2} \end{cases} \quad (4)$$

where, for a given bistable parameterization θ , \blacktriangle_S and \blacktriangledown_S are the water holding strength for the highest attractor of the lower branch and for the lowest attractor of the upper branch, respectively (Fig. 4). In our results, for each year t , we analyze the percentage of ensemble members in the "High runoff coefficient regime". It is defined as the percentage of parameterization θ in the ensemble Θ^* such that $\text{Regime}(S(t)|\theta)$ is the "High runoff coefficient regime".



155 4 Results

4.1 Model calibration

For each watershed, we study the ensemble Θ^* of 1000 parameterizations obtained with the calibration. In Figure 5, we depict the ensemble of simulated runoff coefficients (Fig. 5 **a,b**) and water holding strength (Fig. 5 **c,d**). The starting year of the trajectories differs between each watershed as the initial state value S is computed with the first observed runoff coefficient and Eq. 1. The Sirba and the Dargol watersheds are initialized in 1956 and 1957, respectively (Fig. 5 **a, c**), whereas the Gorouol and the Nakanbé watersheds are initialized in 1961 and 1965, respectively (Fig. 5 **b, d**).

In Figure 5, we observe that until 2014 the four watersheds have increasing trends of runoff coefficients (and decreasing trends of water holding strength, consistently with Eq. 1). This confirms that this simple dynamical model can reproduce the first-order dynamics (the trend) of the observed runoff coefficient. We note that the ensemble mean water holding strength reaches a plateau around the year 1990 for the Gorouol watershed, and around the year 2000 for the Dargol watershed.

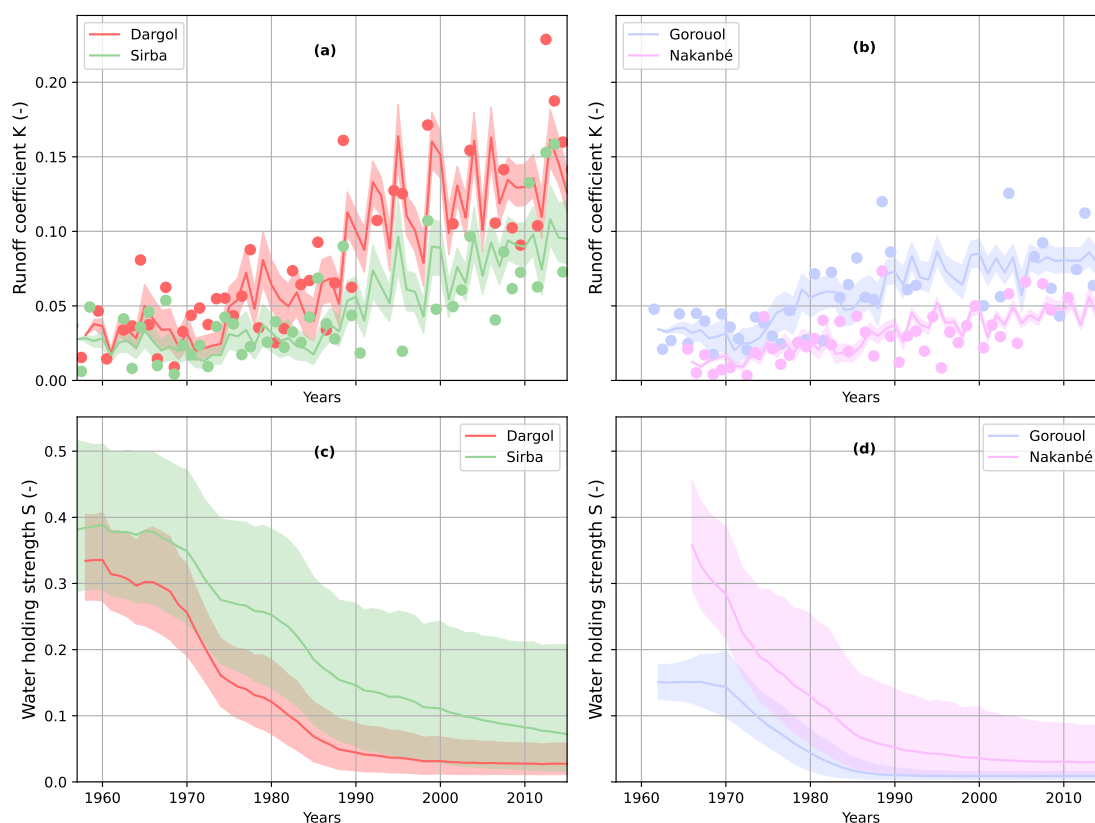


Figure 5. Trajectories of the **(a,b)** runoff coefficient and the corresponding **(c,d)** water holding strength for the four watersheds over the period 1956-2014. The colored line emphasizes the ensemble mean, the colored shaded area highlights the range between quantile 5% and quantile 95% of the ensemble. In the Figure **(a,b)** colored dots designate the runoff coefficient observations, as shown in Fig. 2.



4.2 Bistable parameterizations

Bistable parameterizations represent 90% of ensemble members for the watershed Nakanbé and 100% for the three other watersheds. In Figure 6, for these bistable parameterizations, we illustrate the repartition of $\nabla = (\nabla_P, \nabla_S)$ the lowest attractor of the upper branch and $\blacktriangle = (\blacktriangle_P, \blacktriangle_S)$ the highest attractor of the lower branch. ∇_P and \blacktriangle_P are bifurcation-induced tipping points, i.e. where small changes in annual precipitation can cause a shift to the alternative regime. In general, we find that the repartition of ∇_P , a tipping point for the shift to the high runoff coefficient regime, is less spread than the distribution of \blacktriangle_P , a tipping point for the inverse transition. This is likely because this inverse transition (the decrease of runoff coefficient) was not observed, and thus \blacktriangle_P can hardly be constrained. Lastly, we note that the drier the watershed (see the box plots in Figure 6), the more shifted toward small precipitation values is the distribution of ∇_P .

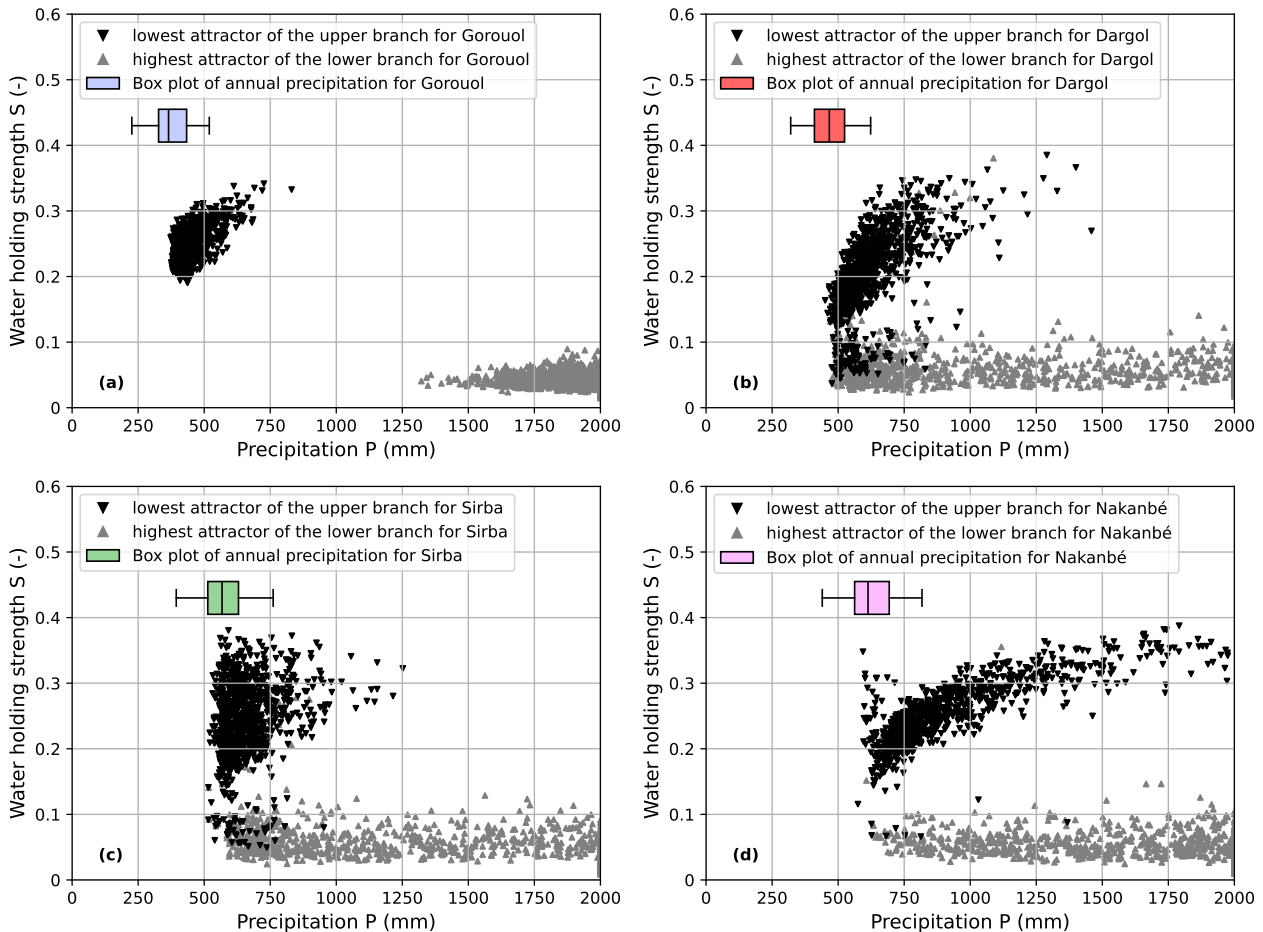


Figure 6. Repartition of ∇ the lowest attractor of the upper branch (in black), and \blacktriangle the highest attractor of the lower branch (in the color of the watershed). For each watershed, lowest and highest attractors of every bistable parameterization of the calibrated ensemble are shown. We also illustrate a box plot (minimum, quantile 0.25, median, quantile 0.75, maximum) of annual precipitation for the period 1965-2014.



175 4.3 Regime shift

We analyze regime shifts between 1965 and 2014, in order to include all watersheds (Nakanbé is initialized in 1965).

In Figure 7, we illustrate the percentage of ensemble members in the "High runoff coefficient regime" (Eq. 4) from 1965 to 2014. In 1965, no ensemble members with bistable parameterizations are in the "High runoff coefficient regime" for the Dargol, Sirba, and Nakanbé watersheds (all ensemble members are in the "Low runoff coefficient regime"). For the Gorououl watershed, 40% of the ensemble members are already in the "High runoff coefficient regime" in 1965. In 2014, more than 85% of ensemble members are in a "High runoff coefficient regime" for all watersheds. Thus, most ensemble members undergo regime shifts: most simulated runoff coefficients belong to the low regime in 1965 and to the high regime in 2014.

To analyze the timing of the regime shift, we define the year of the shift as the first year when strictly more than 50% of ensemble members are in the "High runoff coefficient regime". This regime shift occurred in 1968, 1976, 1977, 1987 for the Gorououl, Dargol, Nakanbé and Sirba watershed, respectively (Figure 7). Then, based on Figure 7, we can also analyze the uncertainty in the regime shift timing, i.e. if all ensemble members are shifting to the "High runoff coefficient regime" altogether or progressively. For Dargol and Nakanbé, the percentage of ensemble members in this regime goes from 0% to 80% in approximately 15 years, while the same increase takes roughly 30 years for the Sirba watershed.

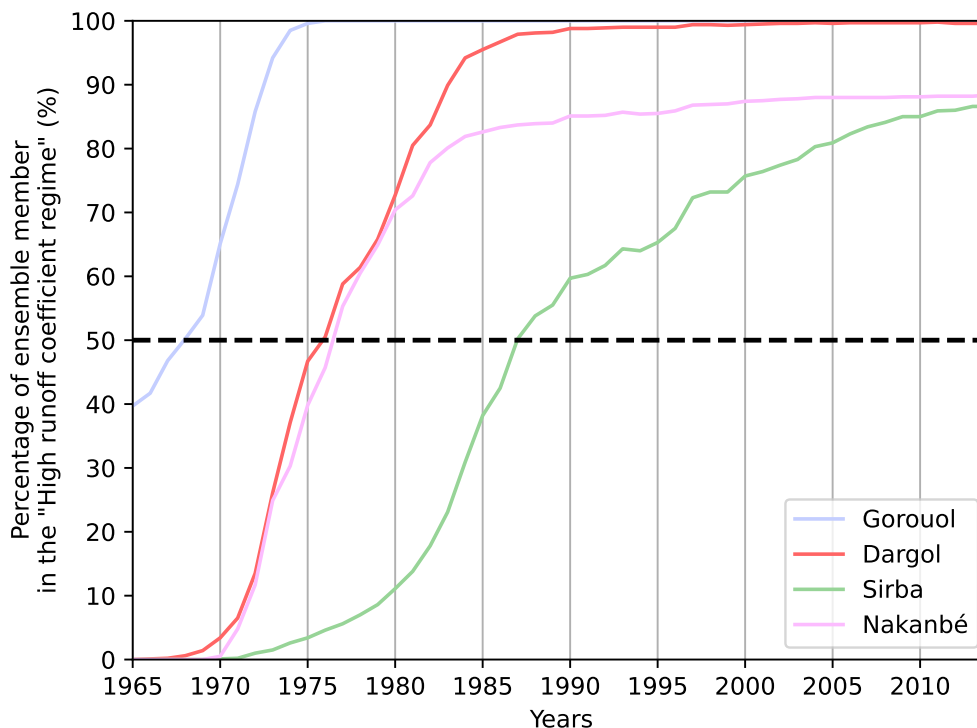


Figure 7. Percentage of ensemble members in the "High runoff coefficient regime" between 1965 and 2014.



5 Discussion

190 The estimated timing of the regime shift depends on several choices such as i) the arbitrary threshold of 50% ensemble members in the "High runoff coefficient regime" to identify a regime shift ii) the proposed definition of separation for the low and high regime, including the choice to calculate attractors until 2000 mm iii) the design of the dynamical model including the choice of external forcing. Indeed, this dynamical model was developed to represent the regime shift as simply as possible. This model, with annual precipitation as unique external forcing, suffices to reproduce a regime shift of runoff coefficients. It has a single
195 forcing, because such models are suited to simulate regime shifts and compute attractors (Scheffer and Carpenter, 2003).

However, adapting our approach to account for several external forcings could improve its realism (at the expense of making calibration more difficult). For instance, in the region, runoff coefficient is known to also largely depends on the precipitation intensity and on the hydrological properties of the watershed, which are impacted by anthropogenic land use changes (Séguis et al., 2004; Descroix et al., 2018; Gbohoui et al., 2021; Yonaba et al., 2021, 2023; Bennour et al., 2023). Furthermore, the
200 dynamical model does not account for the varying influence of temperature on evapotranspiration. All in all, this choice of a single external forcing might explain why the model underestimate the interannual variability of the runoff coefficient (Figure 5), with many observed values outside the range between the quantile 5% and the quantile 95% of the ensemble. However, this limitation does not affect the conclusion of the work, as the model aimed at identifying the timing of regime shift and not precisely reproducing observations. Moreover, despite its simplicity, our results show that it can reproduce the multi-year
205 runoff trend from the annual precipitation alone.

For the Gorouol watershed, we find that the regime shift was around 1968. This result is surprising because before the droughts of the '70s-'80s this watershed did not endure years with a large deficit of annual precipitation, which could have triggered the shift (Figure 2). The main explanation to this timing of regime shift comes from the fact that in 1965 already 40% of ensemble members are, just after their initialization in 1961, in the "High runoff coefficient regime". Each simulated
210 trajectory of the ensemble largely depends on its initial state value S , computed with the first observed runoff coefficient and Eq. 1. Another possibility is that the proposed dynamical model, using only annual precipitation as external forcing, is not adapted to this watershed.

For the Nakanbé watershed, 10% of selected ensemble members are monostable parameterizations, i.e. parameterizations without tipping points. This result suggests that the proposed model is flexible enough to simulate changes in runoff coefficients
215 with or without tipping points. In practice, the single branch of attractors of monostable parameterizations either cover a range of low S values (Fig. 4), or a range containing both low and high S values. In these monostable cases, the increase of simulated runoff coefficients is not induced by a regime shift (abrupt and/or irreversible), but follows the reversible changes in the external forcing (abrupt or not abrupt). To sum up, in our results, the dynamics of simulated runoff coefficients are almost always induced by a regime shift, except in a minority of cases (10% of ensemble members for the Nakanbé watershed) for
220 which the hydrological changes are reversibly adjusted to changes in precipitation.



6 Conclusions

In this article, we assume that the Sahelian paradox (increase in the annual runoff coefficient of Sahelian watersheds during the droughts in the '70s-'80s and after them) is a hydrological regime shift from a low runoff coefficient regime to a high regime, and ask: when did these regime shifts occur? For the Gorouol, Dargol, Nakanbé and Sirba watershed, our results show that
225 Sahelian watersheds shifted during the droughts of the '70s-'80s, with the exception of the Gorouol watershed which may have shifted before. These results depend on several design choices of our two key methodological contributions: the dynamical model and the definition of regimes. Next we summarize these contributions and their potential extensions.

First, we develop a lumped dynamical model driven by precipitation that represents the runoff coefficient of a watershed. This simple model accounts for feedback analogous to the growth and death of vegetation patches. Our results show that
230 the proposed model can reproduce the trend of runoff coefficients, and simulate regime shifts. This model only requires precipitation and runoff data. It could be used on other semi-arid regions, where runoff is mainly due to Horton overland flow, to contribute to the documentation of hydrological regime shifts. Furthermore, a large part of this model is physically interpretable, which is a desirable property for robust extrapolation. Indeed, we could rely on this dynamical model and climate projections to identify watersheds that are likely to experience a regime shift in the future. New model developments would be
235 needed to account for the expected intensification of climatic and anthropogenic pressures on drylands (Wang et al., 2022).

Then, we also propose a novel definition of regimes for bistable parameterizations of the dynamical model. This definition makes it possible to identify regime shifts in the context of transient dynamics, where state values remain far from attractors because the model is too slow to adjust to fast changes in the external forcing. Such quantitative definition of regimes could pave the way to design attribution study for regime shifts, i.e. to assess whether past regime shifts have been made more or less
240 likely by some specific causes, such as anthropogenic emissions.

In the future, the existence of regime shifts in hydrosystems could have direct implications for the adaptation to extreme hydrological events (flood, drought), as well as for water resources management and planning. Indeed, regime shift can lead to unexpected consequences as shown by the Sahelian paradox. In this context, our article proposes two simple contributions toward improving the modelling and characterization of hydrological regime shifts.

245 *Author contributions.* ELR, VW, GP and CP designed the research. ELR performed the analysis and drafted the first version of the manuscript. VW and CP designed the dynamical model. CP ensured the funding acquisition. All authors discussed the results and edited the manuscript.

Competing interests. The authors declare that they have no conflict of interest.

Acknowledgements. This study was funded by the ANR (France) under contract no. ANR-20-CE01-0014-01 (TipHyc project). We thank Patrick Gbohoui for the discharge of the Nakanbe watershed.



250 References

- Armstrong McKay, D. I., Staal, A., Abrams, J. F., Winkelmann, R., Sakschewski, B., Loriani, S., Fetzer, I., Cornell, S. E., Rockström, J., and Lenton, T. M.: Exceeding 1.5°C global warming could trigger multiple climate tipping points, *Science (New York, N.Y.)*, 377, eabn7950, <https://doi.org/10.1126/science.abn7950>, 2022.
- Ashwin, P., Wieczorek, S., Vitolo, R., and Cox, P.: Tipping points in open systems: bifurcation, noise-induced and rate-dependent examples in the climate system, *Philosophical Transactions of the Royal Society A: Mathematical, Physical and Engineering Sciences*, 370, <https://doi.org/10.1098/rsta.2011.0306>, 2012.
- Bennour, A., Jia, L., Menenti, M., Zheng, C., Zeng, Y., Barnieh, B. A., and Jiang, M.: Assessing impacts of climate variability and land use/land cover change on the water balance components in the Sahel using Earth observations and hydrological modelling, *Journal of Hydrology: Regional Studies*, 47, 101–370, <https://doi.org/10.1016/j.ejrh.2023.101370>, 2023.
- 255 Beven, K.: A manifesto for the equifinality thesis, *Journal of Hydrology*, 320, 18–36, <https://doi.org/10.1016/J.JHYDROL.2005.07.007>, 2006.
- Blöschl, G., Bierkens, M. F., Chambel, A., Cudennec, C., Destouni, G., Fiori, A., Kirchner, J. W., McDonnell, J. J., Savenije, H. H., Sivapalan, M., Stumpff, C., Toth, E., Volpi, E., Carr, G., Lupton, C., Salinas, J., Széles, B., Viglione, A., Aksoy, H., Allen, S. T., Amin, A., Andréassian, V., Arheimer, B., Aryal, S. K., Baker, V., Bardsley, E., Barendrecht, M. H., Bartosova, A., Batelaan, O., Berghuijs, W. R.,
- 265 Beven, K., Blume, T., Bogaard, T., Borges de Amorim, P., Böttcher, M. E., Boulet, G., Breinl, K., Brilly, M., Brocca, L., Buytaert, W., Castellarin, A., Castelletti, A., Chen, X., Chen, Y., Chen, Y., Chiffard, P., Claps, P., Clark, M. P., Collins, A. L., Croke, B., Dathe, A., David, P. C., de Barros, F. P., de Rooij, G., Di Baldassarre, G., Driscoll, J. M., Duethmann, D., Dwivedi, R., Eris, E., Farmer, W. H., Feiccabrino, J., Ferguson, G., Ferrari, E., Ferraris, S., Fersch, B., Finger, D., Foglia, L., Fowler, K., Gartsman, B., Gascoin, S., Gaume, E., Gelfan, A., Geris, J., Gharari, S., Gleeson, T., Glendell, M., Gonzalez Bevacqua, A., González-Dugo, M. P., Grimaldi, S., Gupta, A. B.,
- 270 Guse, B., Han, D., Hannah, D., Harpold, A., Haun, S., Heal, K., Helfricht, K., Herrnegger, M., Hipsey, M., Hlaváčiková, H., Hohmann, C., Holko, L., Hopkinson, C., Hrachowitz, M., Illangasekare, T. H., Inam, A., Innocente, C., Istanbuluoğlu, E., Jarihani, B., Kalantari, Z., Kalvans, A., Khanal, S., Khatami, S., Kiesel, J., Kirkby, M., Knoben, W., Kochanek, K., Kohnová, S., Kolechkina, A., Krause, S., Kreamer, D., Kreibich, H., Kunstmann, H., Lange, H., Liberato, M. L., Lindquist, E., Link, T., Liu, J., Loucks, D. P., Luce, C., Mahé, G., Makarieva, O., Malard, J., Mashtayeva, S., Maskey, S., Mas-Pla, J., Mavrova-Guirguinova, M., Mazzoleni, M., Mernild, S., Misstear, B. D., Montanari, A., Müller-Thomy, H., Nabizadeh, A., Nardi, F., Neale, C., Nesterova, N., Nurtaev, B., Odongo, V. O., Panda, S., Pande, S., Pang, Z., Papacharalampous, G., Perrin, C., Pfister, L., Pimentel, R., Polo, M. J., Post, D., Prieto Sierra, C., Ramos, M. H., Renner, M., Reynolds, J. E., Ridolfi, E., Rigon, R., Riva, M., Robertson, D. E., Rosso, R., Roy, T., Sá, J. H., Salvadori, G., Sandells, M., Schaeffli, B., Schumann, A., Scolobig, A., Seibert, J., Servat, E., Shafiei, M., Sharma, A., Sidibe, M., Sidle, R. C., Skaugen, T., Smith, H., Spiessl, S. M., Stein, L., Steinsland, I., Strasser, U., Su, B., Szolgay, J., Tarboton, D., Tauro, F., Thirel, G., Tian, F., Tong, R., Tussupova, K.,
- 280 Tyrallis, H., Uijlenhoet, R., van Beek, R., van der Ent, R. J., van der Ploeg, M., Van Loon, A. F., van Meerveld, I., van Nooijen, R., van Oel, P. R., Vidal, J. P., von Freyberg, J., Vorogushyn, S., Wachniew, P., Wade, A. J., Ward, P., Westerberg, I. K., White, C., Wood, E. F., Woods, R., Xu, Z., Yilmaz, K. K., and Zhang, Y.: Twenty-three unsolved problems in hydrology (UPH)—a community perspective, *Hydrological Sciences Journal*, 64, 1141–1158, <https://doi.org/10.1080/02626667.2019.1620507>, 2019.
- Boyer, J. F., Dieulin, C., Rouche, N., Cres, A., Servat, E., Paturol, J. E., and Mahé, G.: SIEREM: an environmental information system for water resources, in: *Proceedings of the Fifth FRIEND World Conference*, vol. 308, pp. 19–25, IAHS Publications, Cuba, <https://iahs.info/uploads/dms/13630.08-19-25-111-308-Boyer.pdf>, 2006.



- Casenave, A. and Valentin, C.: A runoff capability classification system based on surface features criteria in semi-arid areas of West Africa, *Journal of Hydrology*, 130, 231–249, [https://doi.org/https://doi.org/10.1016/0022-1694\(92\)90112-9](https://doi.org/https://doi.org/10.1016/0022-1694(92)90112-9), 1992.
- Descroix, L., Mahé, G., Lebel, T., Favreau, G., Galle, S., Gautier, E., Olivry, J. C., Albergel, J., Amogu, O., Cappelaere, B.,
290 Dessouassi, R., Diedhiou, A., Le Breton, E., Mamadou, I., and Sighomnou, D.: Spatio-temporal variability of hydrological regimes around the boundaries between Sahelian and Sudanian areas of West Africa: A synthesis, *Journal of Hydrology*, 375, 90–102, <https://doi.org/10.1016/j.jhydrol.2008.12.012>, 2009.
- Descroix, L., Guichard, F., Grippa, M., Lambert, L. A., Panthou, G., Mahé, G., Gal, L., Dardel, C., Quantin, G., Kergoat, L., Bouaïta, Y.,
295 Hiernaux, P., Vischel, T., Pellarin, T., Faty, B., Wilcox, C., Abdou, M. M., Mamadou, I., Vandervaere, J. P., Diongue-Niang, A., Ndiaye, O., Sané, Y., Dacosta, H., Gosset, M., Cassé, C., Sultan, B., Barry, A., Amogu, O., Nnomo, B. N., Barry, A., and Paturel, J. E.: Evolution of surface hydrology in the Sahelo-Sudanian Strip: An updated review, *Water (Switzerland)*, 10, <https://doi.org/10.3390/w10060748>, 2018.
- Dijkstra, Y. M., Schuttelaars, H. M., and Schramkowski, G. P.: A Regime Shift From Low to High Sediment Concentrations in a Tide-Dominated Estuary, *Geophysical Research Letters*, 46, 4338–4345, <https://doi.org/10.1029/2019GL082302>, 2019.
- Favreau, G., Cappelaere, B., Massuel, S., Leblanc, M., Boucher, M., Boulain, N., and Leduc, C.: Land clearing, climate variability, and water
300 resources increase in semiarid southwest Niger: A review, *Water Resources Research*, 45, <https://doi.org/10.1029/2007WR006785>, 2009.
- Feudel, U.: Rate-induced tipping in ecosystems and climate: the role of unstable states, basin boundaries and transient dynamics, *Nonlinear Processes in Geophysics*, 30, 481–502, <https://doi.org/10.5194/npg-30-481-2023>, 2023.
- Fowler, K., Peel, M., Saft, M., Nathan, R., Horne, A., Wilby, R., McCutcheon, C., and Peterson, T.: Hydrological Shifts Threaten Water Resources, <https://doi.org/10.1029/2021WR031210>, 2022a.
- 305 Fowler, K., Peel, M., Saft, M., Peterson, T. J., Western, A., Band, L., Petheram, C., Dharmadi, S., Tan, K. S., Zhang, L., Lane, P., Kiem, A., Marshall, L., Griebel, A., Medlyn, B. E., Ryu, D., Bonotto, G., Wasko, C., Ukkola, A., Stephens, C., Frost, A., Gardiya Weligamage, H., Saco, P., Zheng, H., Chiew, F., Daly, E., Walker, G., Vervoort, R. W., Hughes, J., Trotter, L., Neal, B., Cartwright, I., and Nathan, R.: Explaining changes in rainfall-runoff relationships during and after Australia’s Millennium Drought: a community perspective, *Hydrology and Earth System Sciences*, 26, 6073–6120, <https://doi.org/10.5194/hess-26-6073-2022>, 2022b.
- 310 Gal, L., Grippa, M., Hiernaux, P., Pons, L., and Kergoat, L.: The paradoxical evolution of runoff in the pastoral Sahel: Analysis of the hydrological changes over the Agoufou watershed (Mali) using the KINEROS-2 model, *Hydrology and Earth System Sciences*, 21, 4591–4613, <https://doi.org/10.5194/hess-21-4591-2017>, 2017.
- Gardelle, J., Hiernaux, P., Kergoat, L., and Grippa, M.: Hydrology and Earth System Sciences Less rain, more water in ponds: a remote sensing study of the dynamics of surface waters from 1950 to present in pastoral Sahel (Gourma region, Mali), Tech. rep.,
315 www.hydrol-earth-syst-sci.net/14/309/2010/, 2010.
- Gbohoui, Y. P., Paturel, J. E., Fowe Tazen, Mounirou, L. A., Yonaba, R., Karambiri, H., and Yacouba, H.: Impacts of climate and environmental changes on water resources: A multi-scale study based on Nakanbé nested watersheds in West African Sahel, *Journal of Hydrology: Regional Studies*, 35, <https://doi.org/10.1016/j.ejrh.2021.100828>, 2021.
- Goswami, P., Peterson, T. J., Mondal, A., and Rüdiger, C.: On the existence of multiple states of low flows in catchments in southeast
320 Australia, *Advances in Water Resources*, 187, 104 675, <https://doi.org/10.5281/zenodo>, 2024.
- Hankel, C. and Tziperman, E.: An approach for projecting the timing of abrupt winter Arctic sea ice loss, *Nonlinear Processes in Geophysics*, 30, 299–309, <https://doi.org/10.5194/npg-30-299-2023>, 2023.
- Hastings, A., Abbott, K. C., Cuddington, K., Francis, T., Gellner, G., Lai, Y. C., Morozov, A., Petrovskii, S., Scranton, K., and Zeeman, M. L.: Transient phenomena in ecology, *Science*, 361, <https://doi.org/10.1126/science.aat6412>, 2018.



- 325 Hiernaux, P., Diarra, L., Trichon, V., Mougin, E., Soumaguel, N., and Baup, F.: Woody plant population dynamics in response to climate changes from 1984 to 2006 in Sahel (Gourma, Mali), *Journal of Hydrology*, 375, 103–113, <https://doi.org/10.1016/j.jhydrol.2009.01.043>, 2009.
- Hindmarsh, A. C.: ODEPACK, a systematized collection of ODE solvers, *Scientific Computing*, 1, 55–64, <https://cir.nii.ac.jp/crid/1572543025424393088?lang=en>, 1983.
- 330 Horton, R. E.: The Rôle of infiltration in the hydrologic cycle, *Eos, Transactions American Geophysical Union*, 14, 446–460, <https://doi.org/10.1029/TR014i001p00446>, 1933.
- IPCC: Synthesis Report AR6, Tech. rep., <https://www.ipcc.ch/report/sixth-assessment-report-cycle/>, 2023.
- Kéfi, S., Génin, A., Garcia-Mayor, A., Guirado, E., Cabral, J. S., Berdugo, M., Guerber, J., Solé, R., and Maestre, F. T.: Self-organization as a mechanism of resilience in dryland ecosystems, *Proceedings of the National Academy of Sciences of the United States of America*, 121, <https://doi.org/10.1073/pnas.2305153121>, 2024.
- 335 Lafore, J. P., Flamant, C., Guichard, F., Parker, D. J., Bouniol, D., Fink, A. H., Giraud, V., Gosset, M., Hall, N., Höller, H., Jones, S. C., Protat, A., Roca, R., Roux, F., Saïd, F., and Thorncroft, C.: Progress in understanding of weather systems in West Africa, *Atmospheric Science Letters*, 12, 7–12, <https://doi.org/10.1002/asl.335>, 2011.
- Leblanc, M. J., Favreau, G., Massuel, S., Tweed, S. O., Loireau, M., and Cappelaere, B.: Land clearance and hydrological change in the Sahel: SW Niger, *Global and Planetary Change*, 61, 135–150, <https://doi.org/10.1016/j.gloplacha.2007.08.011>, 2008.
- 340 Lenton, T. M.: Early warning of climate tipping points, *Nature Climate Change*, 1, 201–209, <https://doi.org/10.1038/nclimate1143>, 2011.
- Liu, Q., Yang, Y., Liang, L., Yan, D., Wang, X., Li, C., and Sun, T.: Shift in precipitation-streamflow relationship induced by multi-year drought across global catchments, *Science of the Total Environment*, 857, <https://doi.org/10.1016/j.scitotenv.2022.159560>, 2023.
- Mahe, G., Paturel, J. E., Servat, E., Conway, D., and Dezetter, A.: The impact of land use change on soil water holding capacity and river flow modelling in the Nakambe River, Burkina-Faso, *Journal of Hydrology*, 300, 33–43, <https://doi.org/10.1016/j.jhydrol.2004.04.028>, 2005.
- 345 Mayor, A. G., Bautista, S., Rodriguez, F., and Kéfi, S.: Connectivity-Mediated Ecohydrological Feedbacks and Regime Shifts in Drylands, *Ecosystems*, 22, 1497–1511, <https://doi.org/10.1007/s10021-019-00366-w>, 2019.
- Milly, P. C., Betancourt, J., Falkenmark, M., Hirsch, R. M., Kundzewicz, Z. W., Lettenmaier, D. P., and Stouffer, R. J.: Climate change: Stationarity is dead: Whither water management?, <https://doi.org/10.1126/science.1151915>, 2008.
- 350 Panthou, G., Lebel, T., Vischel, T., Quantin, G., Sane, Y., Ba, A., Ndiaye, O., Diongue-Niang, A., and Diopkane, M.: Rainfall intensification in tropical semi-arid regions: The Sahelian case, *Environmental Research Letters*, 13, <https://doi.org/10.1088/1748-9326/aac334>, 2018.
- Peterson, T. J., Saft, M., Peel, M. C., and John, A.: Watersheds may not recover from drought, *Science*, <https://www.science.org>, 2021.
- Rahimi, M., Ghorbani, M., Ahmadaali, K., Salajeghe, A., and Azadi, H.: Dryland river regime shifts in Iran: Drivers and feedbacks, *River Research and Applications*, 39, 1173–1186, <https://doi.org/10.1002/rra.4138>, 2023.
- 355 Redelsperger, J.-L., Thorncroft, C. D., Diedhiou, A., Lebel, T., Parker, D. J., and Polcher, J.: African Monsoon Multidisciplinary Analysis - An International Research Project and Field Campaign, Tech. rep., 2006.
- Saft, M., Western, A. W., Zhang, L., Peel, M. C., and Potter, N. J.: The influence of multiyear drought on the annual rainfall-runoff relationship: An Australian perspective, *Water Resources Research*, 51, 2444–2463, <https://doi.org/10.1002/2014WR015348>, 2015.
- Scheffer, M. and Carpenter, S. R.: Catastrophic regime shifts in ecosystems: Linking theory to observation, <https://doi.org/10.1016/j.tree.2003.09.002>, 2003.
- 360 Scheffer, M., Carpenter², S., Foley³, J. A., Folke, C., and Walker, B.: Catastrophic shifts in ecosystems, Tech. rep., www.nature.com591, 2001.



- Séguis, L., Cappelaere, B., Milési, G., Peugeot, C., Massuel, S., and Favreau, G.: Simulated impacts of climate change and land-clearing on runoff from a small Sahelian catchment, *Hydrological Processes*, 18, 3401–3413, <https://doi.org/10.1002/hyp.1503>, 2004.
- 365 Trambly, Y., Rouché, N., Paturel, J.-E., Mahé, G., Boyer, J.-F., Amoussou, E., Bodian, A., Dacosta, H., Dakhlaoui, H., Dezetter, A., Hughes, D., Hanich, L., Peugeot, C., Tshimanga, R., and Lachassagne, P.: ADHI: the African Database of Hydrometric Indices (1950–2018), *Earth System Science Data*, 13, 1547–1560, <https://doi.org/10.5194/essd-13-1547-2021>, publisher: Copernicus GmbH, 2021.
- Tucker, C., Brandt, M., Hiernaux, P., Kariryaa, A., Rasmussen, K., Small, J., Igel, C., Reiner, F., Melocik, K., Meyer, J., Sinno, S., Romero, E., Glennie, E., Fitts, Y., Morin, A., Pinzon, J., McClain, D., Morin, P., Porter, C., Loeffler, S., Kergoat, L., Issoufou, B. A., Savadogo, P., Wigneron, J. P., Poulter, B., Ciais, P., Kaufmann, R., Myneni, R., Saatchi, S., and Fensholt, R.: Sub-continental-scale carbon stocks of individual trees in African drylands, *Nature*, 615, 80–86, <https://doi.org/10.1038/s41586-022-05653-6>, 2023.
- 370 van Hateren, T. C., Jongen, H. J., Al-Zawaidah, H., Beemster, J. G., Boekee, J., Bogerd, L., Gao, S., Kannen, C., van Meerveld, I., de Lange, S. I., Linke, F., Pinto, R. B., Remmers, J. O., Ruijsch, J., Rusli, S. R., van de Vijssel, R. C., Aerts, J. P., Agoungbome, S. M., Anys, M., Blanco Ramírez, S., van Emmerik, T., Gallitelli, L., Chiquito Gesualdo, G., Gonzalez Otero, W., Hanus, S., He, Z., Hoffmeister, S., Imhoff, R. O., Kerlin, T., Meshram, S. M., Meyer, J., Meyer Oliveira, A., Müller, A. C., Nijzink, R., Scheller, M., Schreyers, L., Sehgal, D., Tasserou, P. F., Teuling, A. J., Trevisson, M., Waldschläger, K., Walraven, B., Wannasin, C., Wienhöfer, J., Zander, M. J., Zhang, S., Zhou, J., Zomer, J. Y., and Zwartendijk, B. W.: Where should hydrology go? An early-career perspective on the next IAHS Scientific Decade: 2023–2032, *Hydrological Sciences Journal*, 68, 529–541, <https://doi.org/10.1080/02626667.2023.2170754>, 2023.
- Van Nes, E. H. and Scheffer, M.: Implications of spatial heterogeneity for catastrophic regime shifts in ecosystems, *Ecology*, 86, 1797–1807, <https://doi.org/10.1890/04-0550>, 2005.
- 380 van Nes, E. H., Hirota, M., Holmgren, M., and Scheffer, M.: Tipping Points in Tropical Tree Cover: Linking Theory to Data, *Global Change Biology*, 20, 1016–1021, <https://doi.org/10.1111/gcb.12398>, 2014.
- Wang, L., Jiao, W., Macbean, N., Rulli, M. C., Manzoni, S., Vico, G., and Odorico, P. D.: Dryland productivity under a changing climate, <https://doi.org/10.1038/s41558-022-01499-y>, 2022.
- 385 Wendling, V., Peugeot, C., Mayor, A. G., Hiernaux, P., Mougin, E., Grippa, M., Kergoat, L., Walcker, R., Galle, S., and Lebel, T.: Drought-induced regime shift and resilience of a Sahelian ecohydrosystem, *Environmental Research Letters*, 14, <https://doi.org/10.1088/1748-9326/ab3dde>, 2019.
- Yonaba, R., Biaou, A. C., Koïta, M., Tazen, F., Mounirou, L. A., Zouré, C. O., Queloz, P., Karambiri, H., and Yacouba, H.: A dynamic land use/land cover input helps in picturing the Sahelian paradox: Assessing variability and attribution of changes in surface runoff in a Sahelian watershed, *Science of the Total Environment*, 757, 143 792, <https://doi.org/10.1016/j.scitotenv.2020.143792>, 2021.
- 390 Yonaba, R., Mounirou, L. A., Tazen, F., Koïta, M., Biaou, A. C., Zouré, C. O., Queloz, P., Karambiri, H., and Yacouba, H.: Future climate or land use? Attribution of changes in surface runoff in a typical Sahelian landscape, *Comptes Rendus. Géoscience*, 355, 1–28, <https://doi.org/10.5802/crgeos.179>, 2023.
- Zipper, S., Popescu, I., Compare, K., Zhang, C., and Seybold, E. C.: Alternative stable states and hydrological regime shifts in a large intermittent river, *Environmental Research Letters*, 17, <https://doi.org/10.1088/1748-9326/ac7539>, 2022.
- 395